# An imaging photoelectron-photoion coincidence investigation of homochiral 2R,3R-butanediol clusters

*Steven Daly[1,†], Ivan Powis[1,*], Gustavo A. Garcia[2], Maurice Tia[2,‡], Laurent Nahon[2].*

[1] School of Chemistry, University Park, University of Nottingham, NG7 2RD Nottingham, United Kingdom.

[2] Synchrotron SOLEIL, l'Orme des Merisiers, Saint Aubin BP 48, 91192 Gif sur Yvette Cedex, France.

†Current Address: Institut Lumiere Matière, UMR5306, CNRS, Université Lyon 1, 69622 Villeurbanne, France

‡Current Address: Institut für Photonik, Technische Universität Wien, Gußhausstraße 27-29, 1040 Wien, Austria

## Abstract :

We report an experimental investigation of homochiral cluster formation in seeded molecular beam expansions of (2R,3R)-butanediol. Synchrotron radiation VUV photoionization measurements have been performed using a double imaging electron-ion spectrometer in various configurations and modes of operation. These include measurements of the cluster ion mass spectra and wavelength scanned ion yields and threshold electron spectra. Protonated cluster ions ranging up to $n$=7 have been observed and size-selected photoelectron spectra and photoelectron circular dichroism (PECD) have been recorded by velocity map imaging at a number of fixed photon energies. Translation temperatures of the cluster ions have been further examined by ion imaging measurements.

As well as the sequence of protonated clusters with integral numbers of butanediol monomer units, a second series with half-integral monomer masses is observed and deduced to result from a facile cleavage of a butanediol monomer moiety within the nascent cluster. This second sequence of half-integral masses displays quite distinct behaviours. PECD measurements are used to show that the half-integral mass clusters ions do not share a common parentage with whole integer masses. Using an analogy developed with simple theoretical calculations of butanediol dimer structures, it is inferred that the dissociative branching into integral and half-integral ion mass sequences is controlled by the presence of different butanediol monomer conformations within the hydrogen bonded clusters.

# Introduction

Relatively weak intermolecular interactions lie at the root of many chemical processes in nature, and may often be identified in the binding of comparatively small molecules to available receptor sites in a biomacromolecular structure. Chiral recognition, providing additional specificity in these cases, is crucial in terrestrial life which displays extremely marked chiral preferences. Often, at the core of the many interactions involving carbohydrates one finds hydrogen-bonds. In aqueous media there will simultaneously be hydrogen-bonded solvent interactions, so that a deeper mechanistic understanding requires clearly distinguishing these. Solvent free, gas phase clustering studies can therefore contribute insight into the formation of intermolecular H-bonding networks generally, and specifically can be designed to examine chiral dependence.[1,2]

Diols present particular opportunities to examine the interplay between inter- and intra-molecular H-bonding interactions, the latter often acting to stabilise preferred conformations of the isolated species. In a recent theoretical and experimental investigation of ethanediol [3] it was shown how a stable dimer complex can be formed with a network of four intermolecular H-bonds when the two monomer units have specific alternative conformations that differ in the orientation of an OH group; other possible monomer unit conformers disrupt this network and so restrict the number of achieved H-bonding interactions, resulting in higher energy dimers. These most favourable ethanediol monomer conformers both have OCCO backbone conformations with gauche (or anti-gauche) dihedral angles, making them transiently chiral, although intriguingly the stable four H-bonded dimer is achiral.

Moving to longer chain diols, the butanediols can have a permanent configurational chirality. In recent work[4] we have examined how a conformational chirality (similar to that just noted for ethanediol) may compete with the absolute configuration at a now asymmetrically substituted carbon to determine the effective chirality or handedness seen in the frontier electron dynamics. In the present paper we will use photoionization based techniques to examine experimentally clusters (size $n$=2—7) formed from enantiomerically pure (2R,3R)-butanediol monomers, where we may anticipate the formation of H bonding networks somewhat analogous to the ethanediol dimer.

In the context of the present JCP issue on imaging techniques, we develop here the advantages of imaging electron/ion coincidence spectrometers. The so-called iPEPICO[5-7] and i²PEPICO, [8-10] are respectively single and double imaging techniques allowing multiplex angular and radial (energetics) information to be retrieved. Depending on the way these multi-dimensional data are projected and reduced, a very large range of VUV photodynamics issues involving the electron (i.e. ionization) and/or nuclear (i.e. fragmentation) continua can be studied in detail. For instance, when one is mainly interested in the electron spectrum [either via threshold photoelectron spectra[11] (TPES), slow photoelectron spectra (SPES)[12] or VMI-PES] or photoelectron angular distributions,[13] [14,15] the mass filtering offered by iPEPICO allows the removal of any background species or spurious compounds[16] or the disentangling of a mixture of species.[17] Complementary ion imaging capabilities (i²PEPICO) further differentiate the ions with respect to their translational energy (thermal vs cold species for instance).[18,19] Conversely, when one is essentially interested in probing the outcome of chemical reactions or the composition of complex media via mass spectroscopy, i$^{(2)}$PEPICO provides in addition the electron footprint of the various species, in some cases allowing isomers to be identified and differentiated by their PES.[20-22] Of course, i²PEPICO is the ideal tool to study energy (and momentum) correlation between electron and ions in dissociative ionization processes.[23,24]

In the context of clusters and complexes studies, iPEPICO provides a means to retrieve the PES (or TPES) of mass selected clusters either for spectroscopic[25,26] or for thermochemical purposes.[27] This

scheme is also very suitable to retrieve the angular distribution of photoelectrons from mass-selected chiral [28-30] or non-chiral clusters.[31] However, only mass-selection is achieved with the iPEPICO scheme and clear identification of the size of the nascent neutral cluster may be precluded if there are cascading fragmentation processes resulting from dissociative ionizations. In such cases an i²PEPICO setup is potentially more capable, in some cases providing enhanced size-selection of the neutral nascent clusters by allowing the rejection of translationally warmed fragment cluster ion species.[32]

In the present paper, and as described below, we mostly used the DELICIOUS2 iPEPICO apparatus[6] as well as, to a lesser extent, the DELICIOUS3 i²PEPICO apparatus[9] available on the DESIRS beamline at Synchrotron SOLEIL.

## Experimental

Enantiomerically pure (2R,3R)-(-)-butanediol was obtained commercially from Aldrich (97% purity). It is a viscous, colourless liquid with a boiling point of 183.5 °C. It was placed into a stainless steel reservoir inside the first jet chamber and heated to 80 °C. The resulting vapour was seeded into a pressure of either He or Ar in the reservoir and the mixture was allowed to expand into vacuum through a 50 μm nozzle (maintained slightly hotter, 85 °C, to avoid condensation). After traversing a first jet chamber the resulting supersonic molecular beam was collimated by a 0.7 mm skimmer before entering the main spectrometer chamber, where it was crossed at 90 degrees by the synchrotron beam in the interaction region of either the DELICIOUS2[6] or DELICIOUS3[9] electron-ion spectrometer. Electrons and ions produced by ionization are extracted mutually at right angles to the molecular beam and light beam, respectively passing through electron velocity map imaging[33] (VMI) and modified Wiley-McLaren time-of-flight ion optics before finally impacting on their time- and position-sensitive detectors.

Photons were provided by the undulator-based DESIRS vacuum ultraviolet beamline,[34] at the French national synchrotron facility SOLEIL. The beamline delivered pure circularly polarized light ($|S_3| > 0.97$) over the whole energy range. The monochromator slits were merely set to avoid detector saturation, providing typical resolutions of the order of a few meVs. For the low photon energies employed here ($h\nu < 15$ eV), a gas filter upstream the monochromator was filled with 0.25 mbar of Ar to achieve spectral purity at the sample.[35]

During the course of this work we identified two cluster-forming expansion conditions that were used for all results presented here. These require seeding the butanediol vapour into either 1.5 bar backing pressure of He, or 0.5 bar Ar. Coincidence measurements were made at several fixed photon energies (9.7 — 11 eV). Additionally, measurements were made while scanning the photon energy in 5 meV steps using DELICIOUS3. For these scanned measurements the oven/nozzle temperature was raised to 110/120 °C. The monochromator slits were set to provide a photon energy resolution of 5 meV, and horizontal linearly polarized light was used ($S_1$=+1). A photodiode downstream the sample (AXUV from IRD) recorded the photon flux used to normalise the energy curves. The DELICIOUS3 double imaging coincidence scheme was here applied to mass-filter the photoelectron images, taking into account only ions coming from the molecular beam, i.e. having a net velocity along this direction. Moreover, and to further minimize the false coincidences background, for each mass only ions having a compatible kinetic energy ($0 < iKE < 0.25$ eV, as defined by their position and TOF) are taken into account. The maximum *iKE* value is chosen so that all ions for any given mass are included, but of course ions having a different mass will be effectively excluded. The procedure is especially efficient

above the monomer's ionization energy (IE), and greatly increases the signal-to-noise ratio for cluster signal by removing the monomer's noise. After removing the false coincidence background, the photoelectron images were converted to threshold electron counts by applying a subtraction method previously described.[6,11] The parameters used for this operation were chosen so as to provide an electron resolution of 50 meV with an extraction field of 35 V/cm.

## Results

Figure 1 shows ion time-of-flight mass spectra recorded for clustering molecular beam expansions of 2,3-butanediol (**BD**) in He and Ar carrier gas at a photon energy of 9.7 eV. This lies just above the monomer ionization threshold (9.68$\pm$0.01 eV), but well below any fragmentation channels of the monomer.[36] Cluster peaks corresponding to $n$-mer species, (**BD**)$_n$ , are clearly evident at integral multiples of the monomer mass (m/z=90), for $n$ ranging up to 7 in the more strongly clustering argon expansion conditions. Less clustering ($n \leq 3$) is evident in the helium expansion. We note that the greater jet velocity along the forward beam direction acquired by species seeded in helium can lead to some systematic discrimination against much heavier masses. With longer flight times these will experience a greater transverse displacement, possibly exceeding the detector's physical dimension, before reaching the end of the ion drift region. Such an increasing displacement of heavier ions towards the detector circumference could be observed in the ion images. In practice, therefore, for the faster helium expansion a deflecting field was applied in the ToF drift region to steer the ions back towards the detector centre.

Perhaps less expected are the additional mass peaks, (**BD**)$_{n+\frac{1}{2}}$ , appearing at half-integer monomer mass multiples in both expansions. Formation of these must necessitate some C-C bond cleavage, which in the pure monomer cation has been shown to require at least 0.48 eV in excess of the ground electronic state ionization threshold.[36] We will refer to these quite generally as the $n\frac{1}{2}$-mers. The first two members of this series ($n$= 1½, 2½) are more intense than their adjoining integer $n$-mer peaks in both argon and helium expansions at $h\nu$=9.7 eV. In argon expansion the $n$=3½ peak is of comparable intensity to the adjacent $n$-mers, and even higher members of this sequence, up to $n$=6½ can be detected.

Very little fragmentation is seen at sub-monomer masses in Fig. 1, unsurprisingly since $h\nu$=9.7 eV lies below any fragmentation channel thresholds established for the pure monomer ionization.[36] Traces of m/z=44,45 fragments (the dominant monomer cleavages with appearance energy of 10.3 eV) are seen, but a hint of their formation mechanism is provided by the adjacent m/z=40 peak seen in the argon expansion. This must be Ar$^+$ ion resulting from ionization by residual second order synchrotron radiation. For these measurements a 0.25 mbar argon gas filter was used downstream of the monochromator to attenuate second order light above the argon IE by a factor of ~1000, but there is evidently sufficient remaining to ionize some argon (but not helium) carrier gas and so also to generate a trace of more energetic dissociative ionization of the butanediol.

At higher photon energies (not shown here) more sub-monomer mass fragments begin to appear in the ToF mass spectrum as the m/z 72,75 and m/z 44–47 fragmentation thresholds of the monomer ion[36] are reached. At the same time the higher $n$-mer peaks slowly decrease in relative intensity while the $n\frac{1}{2}$-mer sequence also becomes less intense relative to the $n$-mer sequence.

In Figure 2 the first few $n$-mer and $n\frac{1}{2}$-mer peak regions seen in Fig. 1 are displayed with an expanded mass scale. Immediately it is seen that the 1-mer feature is actually a doublet consisting of

a parent mass peak (m/z 90) and a smaller (m/z 91) peak that must be mainly a protonated monomer unit (since at natural abundance the $^{13}C$ isotope would only account for 4.4% of the m/z 90 signal). The nominal 2-mer feature is seen to be predominantly a protonated dimer (m/z 181), with now a weaker contribution of the genuine dimer mass (m/z 180) while the nominal 3-mer is dominated by a broadened peak centred at the protonated trimer mass (m/z 271). Although not shown, the higher $n$-mer features are similarly broadened and increasingly asymmetric peaks (tailing to longer flight time) and are centred at the protonated $n$-mer masses. Although for convenience we shall retain the nominal $n$-mer labelling to designate cluster size, the presence of protonated species ($n\times90 + 1$ amu) is a clear indication that many of the $n$-mer ions must be produced following fragmentation from heavier clusters — of size at least $n+1$ monomer units.

Of course this must also apply to parentage of the $n\frac{1}{2}$-mer species. Examining now these regions of the ToF mass spectra (Fig. 2) the $n=1\frac{1}{2}$ feature is seen to comprise a principal peak at m/z 135 ($1\frac{1}{2}\times90$ amu) and a secondary, weaker m/z 136 peak. While visually similar to the $n=1$ region, a greater width of the peak pairs is noticeable, possibly indicating a greater translational temperature for these ions.  The $n=2\frac{1}{2}$ mass region predominantly consists of a single, relatively narrow peak at m/z 225 ($2\frac{1}{2}\times90$ amu). Finally the major contribution to the nominal $n=3\frac{1}{2}$ region is a peak at m/z 315 (again exactly $3\frac{1}{2}\times90$ amu), but now with some additional mass in the m/z 316—318 range.  It may be concluded that the $n\frac{1}{2}$-mers are dominantly formed from their parent neutral by loss of a m/z 45 fragment plus an as yet unspecified number of whole monomer mass units.

In Figure 3 we show the results of threshold photoelectron-photoion coincidence (TPEPICO) ion yield scans made between $h\nu$=8.4 eV and $h\nu$=10.5 eV using a 0.6 bar argon expansion. The detected ion count has been sorted into separate channels centred on the $n$-mer and $n\frac{1}{2}$-mer mass peaks, filtered to accept only ions coincident with (near-)zero energy electrons, and normalised by photon flux. TPEPICO thus achieves internal energy selection such that the ionization energy of the various species is well-defined by the photon energy (to within the resolution of the threshold electron filtering — here relaxed to 50 meV in order to maintain reasonable statistical data quality). *Appearance energies have now been estimated by extrapolating the straight line rise in yield to the baseline, and these values are included in Table 1.*

Alternatively, these TPEPICO curves can be viewed as size-selected threshold electron spectra (TPES) and so it is convenient to compare at the same time dispersed photoelectron spectra obtained by the inversion of fixed wavelength velocity mapped electron images (VMI-PES). These have been recorded at a number of fixed photon energies between 9.7 and 11.0 eV.  Figure 4(a) (top panel) shows the size-selected coincident VMI-PES recorded at $h\nu$=11.0 eV in a 1.5 bar He expansion, which proves quite similar to the Fig. 3 TPES. All spectra in Figs. 3 and 4 have been individually normalised to facilitate comparisons. It should be noted that the S/N of the weak $n=3\frac{1}{2}$ TPEPICO/TPES signal makes this unreliable above $h\nu\approx9.5$ eV where false coincidences with the much more intense monomer electrons present in the same energy region become problematic.

The $n=1$ TPES and VMI-PES appear as a relatively narrow band, essentially identical to the first band VMI PES recorded in non-cluster forming conditions (Figure S3 Supplementary Material of  Ref. [4]). More particularly, the TPES onset, 9.69±0.01 eV (Table 1), is fully consistent with that (9.68 ±0.01 eV) determined in non-clustering conditions.[36] The VMI-PES onset appears a little lower, although this is attributable to the smearing consequent on the lower energy resolution achieved in this mode. The $n$=2, 3, and (TPES only) $n$= 4 TPES/VMI-PES onsets are seen to be clearly size-specific, successively

displaced to lower threshold values. Such monotonic reduction in ionization threshold correlating with increased cluster size is qualitatively expected behaviour. These higher $n$-mer photoelectron bands are also seen to become much broader than that of the $n$=1 feature, extending in both directions to higher and lower energy.

The $n\frac{1}{2}$-mer TPES/VMI-PES bands are each quite distinctive and qualitatively different from the $n$-mers, being much more narrowly peaked (to increasingly lower energy) than the higher $n$-mers. The $n\frac{1}{2}$-mer peak onsets are even more strongly displaced to lower energies than the next adjacent $(n+1)$-mer. These observations provide a first suggestion that the $n$-mer and $n\frac{1}{2}$-mer sequences are somehow distinct and not simply interleaved daughter fragments sharing a common parent cluster sequence. At the higher fixed photon energy (11 eV) of the VMI-PES recording in Fig. 4(a) there is additionally some production of $n$=½ fragment requiring a C-C bond cleavage in a monomer unit. This has an onset that is fully consistent with the 10.32 eV appearance energy previously determined from the **BD** monomer.[36]

Fig. 4(b) (lower panel) shows the VMI-PES recorded in a more strongly clustering Ar expansion and at a 10.0 eV photon energy which is set, therefore, above the monomer adiabatic threshold, but below the monomer fragmentation thresholds. The relative displacement of the rising edges of the $n$-mer VMI-PES bands clearly show the expected monotonic decrease in ionization energy accompanying increasing cluster size and so suggests a distinct 1:1 mapping between ionization mechanism and production of a given $n$- cluster ion. A similar correlation is seen for the $n\frac{1}{2}$-mers, but the two sequences do not simply interleave, as already noted. However, close to the thresholds, at low intensity, the behaviour can switch; the $n$=3, 4, 5 and the $n$=6, 7 data curves seemingly converge to two common onsets. Now the $n$=2 VMI-PES proves particularly enlightening. Back extrapolation of the rising edge of this curve suggests it should cut the baseline at a value intermediate between the $n$=1 and $n$=3 neighbours. In fact, as the expanded inset to Fig. 4(b) shows there is a low intensity/low energy pedestal such that the curve deviates and converges instead towards the $n$=3 onset. The same pedestal is seen in the 1.5 bar He expansion conditions and is even more prominent in the $h\nu$=9.7 eV measurement, but is not noticeable at $h\nu$=10.5 eV or above.

In Supplementary Material we provide PEPICO mode ion yield scan curves, made without any electron energy selection, and hence lacking any ion internal energy selection. On the other hand the increased statistics allows for closer examination of the very shallow, low intensity threshold regions. As discussed there, there is now some suggestion of near threshold instability in heavier mass channels, presumably of a minor, thermally hot component, that causes their further fragmentation into lighter mass $n$-mers. Cascading means that ultimately all such $n$-mer production ($n$= 2 —7) tends towards a common observed threshold of 8.73 ±0.06 eV.

Cluster size-selected velocity map ion images were obtained by filtering against the ion ToF information in the Ar clustering expansion conditions. Measurements were made both at fixed photon energies (9.7 eV, 10.0 eV, and 10.2 eV) and also while the photon energy was scanned through the sub-monomer ion threshold region 8.9 —9.4 eV. Kinetic energy release distributions (KERDs) were developed from these images using each ion's detector impact position ($x$, $y$) and precise timing ($t$) to establish its 3D velocity ($v_x$-$v_{MB}$, $v_y$, $v_z$ ). Note that the mean value of the $v_x$ component (along the molecular beam) also carries the information on the molecular beam's velocity, $v_{MB}$, which is measured at close to 600 m s$^{-1}$ in the Ar expansion. The KERDs were all well-fitted by a Boltzmann distribution function.

Figure 5 presents fitted Boltzmann 3D translational temperatures obtained for the ion images recorded with scanned 9.15±0.25 eV photon energies, that is below the true monomer adiabatic ionization energy. The $Ar^+$ ions ($2^{nd}$ order light) have a translational temperature of 47 K which we therefore take as that of the molecular beam. The size-selected (m/z 90+91) $n$=1 butanediol component is slightly warmer (59 K). While this might indicate that molecules seeded in the beam aren't so efficiently cooled, it may also result as warming by energy release in the fragmentation from larger size clusters as direct ionization is not here energetically feasible. All other species are significantly translationally hotter, again we suppose reflecting an increased energy release in fragmentation to $BD_n \cdot H^+$ and $BD_{n+\frac{1}{2}}{}^+$, but the $n\frac{1}{2}$-mers appear consistently cooler than their neighbouring $n$-mer ions. However, with increasing size all the clustered species tend asymptotically towards a translational temperature of ~120 K.

These measurements were all made with a pure (2R,3R)-butanediol enantiomer sample; in consequence it is reasonable to expect that the clusters will also be chiral. Finally, therefore, we examined size-selected photoelectron circular dichroism (PECD) in these clustering conditions by recording alternating VMI-PES images using Left and Right circularly polarized synchrotron radiation.[37] The photoelectron angular distribution in the dichroism images (LCP-RCP) recorded in coincidence with a given cluster size is then extracted, to provide a measure of the chiral asymmetry which is quantified as $b_1^{\{+1\}}$, the coefficient of the odd cosine term in the distribution function. Further information and example size-selected electron VMI images are included in Supplementary Material. The mean $b_1^{\{+1\}}$ results obtained are shown, as functions of cluster size and photon energy, in Figure 6.

PECD is known to provide a structure dependent chiral signature that reflects the final state scattering of the outgoing photoelectron by the chiral molecular (cluster) potential.[14] As such it is expected to be indicative of the nascent molecule or cluster structure, molecular fragmentation being a much slower process occurring after the ionization step. PECD may thus help in identifying the origin of the $n$-mers vs $n\frac{1}{2}$-mers. From Fig. 6 it is seen that the mid-range $n$-mers display rather similar chiral asymmetries that increase slightly with increasing ionization energies. The variability with photon energy increases for the largest $n$-mers, and more markedly for the 1-mer. As in previous investigations of camphor dimerisation[29], epichlorohydrin clustering[28] and glycidol clustering,[30] significant differences in PECD can be detected between the monomer, dimer and to a less extent higher $n$-mers.

The $n\frac{1}{2}$-mer PECD does not appear to conform to the same trends; certainly the $n$=3½ and, especially, the $n$=2½ species have a very different photon energy dependence, as compared to their adjacent $n$-mers, suggesting these species originate from distinctly different parents than do the $n$-mers. Notably, all the species present in the jet exhibit non-vanishing PECD showing that they all present a chiral structure.

## Discussion

It is natural to expect that there will be an excess of unclustered monomer in the cold molecular beam such that under most conditions the majority of $n$=1 ion results from simple monomer ionization. The $n$=1 mass spectrum at $h\upsilon$=9.7 eV, very close to the monomer ionization threshold, is dominated by $BD^+$ ions (Fig 2) and even under normal coincidence recording conditions the mass resolution remained high enough that m/z 90 could be selected, rejecting the protonated m/z 91

component. The small amount of **BD·H⁺** seen at $h\nu$=9.7 eV must result from larger clusters (with a lower ionization threshold), but can be expected to be of diminishing relative importance at higher photon energies as the monomer ionization cross section increases. Figure 7 examines the PECD photon energy dependence of $n$=1 more closely. It can be seen that the chiral photoelectron anisotropy parameters, $b_1^{\{+1\}}$, under both He and Ar clustering expansion conditions are in excellent agreement, but are also effectively identical to an earlier monomer measurement made under non-clustering conditions.[4] PECD can be extremely sensitive to the parent neutral structure,[14] and hence to nascent cluster size. In the case of glycidol, for example, the PECD signal even changes sign between the monomer and dimer species.[30] Consequently, one can be confident that above the monomer ionization threshold the dominant $n$=1 ionization is from pure monomer neutral.

Even at a photon energy barely above the monomer appearance energy (Fig. 1) an extensive series of cluster ions are detected. It is of course reasonable to expect that intermolecular interactions in a given size cluster will be enhanced in the more strongly polarizing charged cation environment, thereby conferring increasing stability on the ion. Correspondingly, one therefore can expect a reduction in the cluster ionization potential relative to the monomer. In previous cluster ion studies of acetone,[38] NO,[39] CS$_2$,[40] and epichlorohydrin[28] it has been found that plotting ionization energy against 1/$n$, for cluster sizes $n$ that range as high as 7, produces a simple linear correlation. Figure 8 shows an application of this simple model to 2,3 butanediol clusters, using the TPES appearance energies (Table 1) and, alternatively VMI-PES data. For the latter we have obtained consistent estimates of the *relative* ionization energy by recording the electron energy 50% up the rising edge of the PES band (similarly as for the epichlorohydrin study[28]). While not shown here, essentially similar plots are obtained from the VMI-PES measured at different photon energies.

These 1/$n$ plots produce rather astonishingly good straight line fits with two caveats; the $n$-mer and $n\frac{1}{2}$-mer sequences must be treated separately, and the $n$=1 data points do not fall close to an extrapolation from the other $n$-mer sequence members. A linear 1/$n$ functional dependence of an ionization energy was first rationalised[38] using a simple Huckel-like quantum mechanical model in which the monomer orbital levels are perturbed only by weak near-neighbour interactions in the cluster. Applying such an interpretation here would be problematic for the half-integral clusters, but more generally it is evident from the ion mass (Fig. 2) and kinetic energy (Fig. 5) studies that most of the observed clusters $n$>1 result from dissociative ionization of larger neutral clusters. Hence, the appearance energies must depend on both ionization and ion fragmentation energetics. Of course, if the bond breakage energetics leading to **BD$_n$·H⁺** were relatively size independent, this might simply appear as a constant offset to the linear curve derived from ionization energy alone. Following this thought, we can note that offsetting the $n$-mer fitted line in either panel of Fig. 8 by ~0.6 eV would bring the $n$=1 true monomer datum (ionization with no fragmentation) into line.

The good 1/($n+\frac{1}{2}$) linear correlation displayed by the $n\frac{1}{2}$-mers is even further removed from the rationalisation offered by the simple size-dependent ionization model, [38] which requires integer $n$. Also included in Figure 8 are plots of the data against 1/$N$, where $N$ is taken to be the next highest integer from $n$, and hence represents the smallest neutral cluster that could be dissociatively ionized to give the observed ionic clusters. Equally impressive linear behaviour is found with this alternative model, and one cannot meaningfully choose between them. But taking a purely phenomenological view of Fig. 8, it distils the observations from the wavelength scanning measurements described in the Results section that the $n$-mer and $n\frac{1}{2}$-mer sequences do not simply interleave. Of course the

required fragmentation energies from the nascent cluster ion parents can be expected to differ for the two series. Apart from the simple argument, above, that suggests perhaps 0.6 eV to fragment to **BD·H⁺** there are no indications as to what the neutral species cleaved off in the *n*-mer sequence may be. Cleavage of the central C(2)-C(3) bond, producing m/z 47—44 ions (dominantly m/z 45) is seen in the monomer ionization some 0.48—0.64 eV above the monomer ionization onset, and while such cleavage would seem likely to be somehow implicated in the *n*½-mer series, the energetic threshold seems surprisingly high for the clusters at low photon energy.

Although a full theoretical modelling of this complex system is beyond the scope of the present paper, some insight may be had from a non-exhaustive study of H-bonding networks in the dimer alone. A description and discussion of the monomer conformers, their likely population under rapid cooling in a molecular beam expansion, and expectations for dimer formation is provided as Supplementary Material. Figure 9 summarises our results, illustrating the two most stable neutral dimer structures we computed at the MP2/6-311++G(d,p) level.  The most stable (G′G′) dimer structure comprises two identical monomer units both having anti-gauche (G′) OCCO backbone conformation. The next lowest energy dimer (GG′) is built from mixed gauche/anti-gauche monomer units. Both these dimer conformations are stabilised by formation of networks of 4 H-bonds and they differ in energy by less than 1.9 kJ mol⁻¹. They are plausibly both likely in the molecular beam environment.

The G′ monomer cation structure has an extended (1.998 Å) one-electron central C-C bond.[36] In the lower part of Fig. 9 we show an optimised cation structure (unlikely to be unique) for the G′G′ dimer, and its singly occupied HOMO. This is fairly described as **BD·BD⁺** and the ionized monomer moiety in the dimer, like the monomer ion, has an extended central C-C bond (2.03 Å). Despite this weakened central bond, the symmetric fragmentation of the monomer ion requires a significant fraction of an eV more energy. However, we may observe that in the monomer symmetric fragmentation requires not only cleavage of the central carbon linkage, but also the rupture of the intramolecular H-bond that confers stability on the G′ structure. In contrast, the G′G′ cation structure shown in Fig. 9 at least retains a single H-bond. Such one-electron bonds and H-bridged structures are not without precedent in vicinal diols having been identified as global minima on the cation potential surface in studies of 1,2 ethanediol[41] and 1,2 propanediol.[42] Even in 2,3 butanediol, rearrangement to a dimeric H-bridged $(CH_3CHOH)_2^+$ structure exceeds the direct ionization by only 7.8 kJ mol⁻¹.[36]

In contrast to the G′G′ cation structure, the GG′ cation structure retains the neutral H-bonding network, but is not shown in Fig 9 as it looks similar to the neutral. It is not, however, difficult to visualise the (G′G′)⁺ structure shown in Fig. 9 as a transition state for fragmentation of an ionized **BD₂** dimer to the *n*=1½ cation detected in our experiments.

Finally, we examine the experimental PECD data. A major part of the chiral asymmetry in electron angular distribution that is detected by a PECD measurement derives from the scattering of the outgoing photoelectron off the chiral molecular potential.[14,43] An interesting comparison can be drawn with earlier studies of glycidol. Both glycidol[44,45] and 2,3**BD**[4] monomers have been found to have strongly conformer-specific PECD. Even more dramatic cluster size differences were found in glycidol cluster ionization, there being a complete inversion of the asymmetry that occurs between glycidol monomer and glycidol dimer.[30] Differences observed between the PECD for larger glycidol cluster sizes were more subtle, though reproducible.  In Fig. 6 it may also appear that for the mid-sized *n*-mer clusters of butanediol the PECD is less strongly size-dependent. Besides the inherent sensitivity of PECD to the photoelectron scattering off the long-range molecular potential, and

therefore on the clustering itself, a further relevant factor influencing these behaviours may be whether a given cluster size possesses a single well-defined structure or not. As discussed for the 23**BD** dimer, above, it could be that different monomer conformations are involved and alternative H-bonding networks could exist within stable members of a given cluster size.

In the **BD** cluster PECD results (Fig. 6), $n$=2½, 3½ results clearly stand apart from the trends established by the $n$-mer series; the $n$=1½ PECD characterisation is perhaps more ambiguous. In Fig. 7 we have plotted out the photon energy dependent $n$=2 and 2½ PECD parameters for a more direct comparison with each other and with the monomer PECD results. The timescale for departure of the photoelectron can be expected to be much faster than that of any nuclear dynamics, and hence PECD should be indicative of the neutral's nuclear configuration at the point of ionization. It might be expected that ionized **BD**$_2$·**H**$^+$ or **BD**$_{2½}^+$ could be descendants from a common neutral parent, perhaps **BD**$_3$, yet from the distinct PECD there can be no doubt that the nascent neutral structures leading to the $n$=2 and $n$=2½ cluster ion species are totally different, as the photoelectron spectroscopy shown in Figs. 3-4 suggested. Although the monomer conformer **I** can be identified as the $n$=1 precursor, from the excellent agreement between the experiment and conformer **I** calculated PECD, a similar identification of the $n$=2, 2½ precursors will require more theoretical guidance than is currently available.

As seen in Fig 7, for $n$=1, 2 there is effectively no difference between PECD recorded in He and Ar clustering beams, the measurements being identical within the error bars for these conditions. For $n$=2½, however, the colder He beam evidently produces somewhat greater asymmetry above $h\nu$ = 10.4 eV. A similar observation was noted, and more extensively investigated, in the glycidol cluster PECD studies.[30] There it was possible to infer that in the more strongly clustering Ar beam there was some cascading fragmentation from a broader range of larger neutral clusters to a given ionic cluster, with a consequent attenuation of the mean PECD that could be observed. Further investigation may be desirable here, but in light of the shallow, converging threshold behaviours noted in the Ar cluster beam in both the mass-selected PEPICO ion yields (see Supplementary Material) and VMI-PES (Fig. 4b) it seems likely that some cascading from larger neutrals to mid-range $n$-mer cluster ions does occur here too.

## Conclusions

We have reported a range of measurements made using synchrotron VUV radiation at the DESIRS beamline of the French national synchrotron SOLEIL, using the double imaging DELICIOUS electron-ion spectrometer in various configurations and modes of operation. Foremost amongst our findings is the observation of a strong sequence of cluster ions with half integral monomer masses ($n$½-mers), accompanying the expected series of integral $n$-mers. Many of the observations made here argue against these alternatives being a result of either competitive or sequential fragmentations from any common parent cluster cations. Most telling are the photoelectron circular dichroism (PECD) measurements. These can be expected to carry a signature of the nascent ionization, before any fragmentation, and so to vary with cluster size and conformation. The $n$=2½, 3½ (and probably also $n$=1½) ions' PECD is quite distinct from any of the observed $n$-mer series PECD up to $n$=7 allowing us to infer a quite distinct structural parentages for the $n$½-mer series.

It is unlikely that it is simply cluster size that differentiates the $n$-mer and $n$½-mer precursors, since to have unique sized parents for all members of both $n$-mer and $n$½-mer sequences logically requires an even larger range of neutral cluster sizes to be present in the cluster beam. This leaves us to infer that the distinctive alternative $n$- and $n$½- fragmentation pathways are most probably attributable to different monomer conformations within the clusters. While we are not able to present detailed

theoretical modelling to corroborate this, a simpler calculation on the alternate G'G' and G'G dimer structures, somewhat analogous to the alternative structures experimentally observed in glycidol dimer molecular beams,[46,47] provides some strong hints as to how the incorporation of different monomer conformers into a given size cluster may act to control the preferred cluster fragmentation.

Upon closer examinations the heavier $n$-mer species ($n \geq 3$) detected are found typically to be protonated clusters, with some accompanying translational energy warming, presumably produced by dissociative photoionization of larger neutral clusters. Energetic thresholds for each $n$-mer channel have been observed in the ion yields recorded while scanning photon energy, and also by recording VMI photoelectron spectra at fixed wavelengths. These energetics show a clear monotonic decrease with increasing cluster size. Perhaps surprisingly, the thresholds display a very linear variation with the inverse of the cluster size, but the significance of this is less clear here than in previous cluster ion studies noted.[28,38-40] Right at threshold, many of these $n$-mer channels have very weak, shallow onsets that seem to tail below the extrapolated channel-specific threshold towards that of heavier clusters, up to $n=7$; this is a likely indicator of cascading fragmentation from neutral clusters that are more than a single monomer unit (m/z = 90) heavier than the nominal cluster ion size, $n$. Conversely, much of the available evidence tends to suggest that above threshold for each cluster ion, $n$, the dominant channel is quite well delineated and distinguishable from its neighbours.

More obviously, generation of members of the $n\frac{1}{2}$ sequence suggests that a monomer unit in the cluster has cleaved off a fragment at its central C(2)-C(3) bond. Such fragmentation is the dominant channel in the monomer[36], but there it requires around half an eV excess energy. On the other hand $n\frac{1}{2}$-mer cations are observed here seemingly much closer to the supposed ionization thresholds, making such a large excess for the fragmentation seem improbable. A possible resolution of this paradox is that the monomer fragmentation requires cleavage also of an intramolecular H-bond, whereas in the cluster ions the H-bond can be switched to an intermolecular one, which is thus retained and helps binding of the cluster cation.

Despite the richly detailed array of experimental data that we have assembled on these butanediol cluster ions there are many open questions regarding the behaviour and stability of the clusters. Additional experimental investigations can readily be identified for further studies, but most importantly there is a need for guidance from a theoretical investigation of the homochiral neutral and cation H-bonded structures that can be formed in molecular beam expansions of 2,3 butanediol.

## Supplementary Material

See supplementary material for PEPICO ion yield scan data, further information on the VMI PES/PECD analysis, and details of the calculations of possible dimer structures.

## Acknowledgements

**Table 1** Appearance energies for principal 2,3 butanediol cluster features, determined from TPEPICO/TPES scans

|        | Appearance Energy [a] (eV) |              |
|--------|----------------------------|--------------|
| 1-mer  | 9.69 ± 0.01                |              |
| 1½-mer |                            | 9.27 ± 0.01  |
| 2-mer  | 9.41 ± 0.01                |              |
| 2½-mer |                            | 8.93 ± 0.05  |
| 3-mer  | 9.09 ± 0.02                |              |
| 3½-mer |                            | 8.76±0.04 [b] |
| 4-mer  | 8.94 ± 0.02                |              |
| 5-mer  | 8.87 ± 0.05                |              |

[a] Obtained by linear back extrapolation to the baseline. The stated uncertainty represents the precision of baseline intercept, read from the photon energy scale. Because "threshold" electron detection here includes a hot electron tail (to 50 meV) to secure good statistics, the quoted photon energy values will represent upper limits to the true energetic thresholds.

[b] linear extrapolation could not be applied due to low S/N, instead this value was read by eye.

# References

1    A. Zehnacker, *Chiral Recognition in the Gas Phase*. (Taylor & Francis, Boca Raton, US, 2010).
2    A. Zehnacker and M. A. Suhm, Angew. Chem.-Int. Edit. **47**, 6970 (2008).
3    F. Kollipost, K. E. Otto, and M. A. Suhm, Angew. Chem.-Int. Edit. **55**, 4591 (2016).
4    S. Daly, M. Tia, G. A. Garcia, L. Nahon, and I. Powis, Angew. Chem.-Int. Edit. **55**, 11054 (2016).
5    P. Downie and I. Powis, J. Chem. Phys. **111**, 4535 (1999).
6    G. A. Garcia, H. Soldi-Lose, and L. Nahon, Rev. Sci. Instrum. **80**, Art. no. 023102 (2009).
7    A. Bodi, M. Johnson, T. Gerber, Z. Gengeliczki, B. Sztaray, and T. Baer, Rev. Sci. Instrum. **80** (2009).
8    A. Vredenborg, W. G. Roeterdink, and M. H. M. Janssen, Rev. Sci. Instrum. **79**, 063108 (2008).
9    G. A. Garcia, B. K. C. de Miranda, M. Tia, S. Daly, and L. Nahon, Rev. Sci. Instrum. **84**, 053112 (2013).
10   A. Bodi, P. Hemberger, T. Gerber, and B. Sztaray, The Review of scientific instruments **83**, 083105 (2012).
11   B. Sztaray and T. Baer, Rev. Sci. Instrum. **74**, 3763 (2003).
12   J. C. Poully, J. P. Schermann, N. Nieuwjaer, F. Lecomte, G. Gregoire, C. Desfrancois, G. A. Garcia, L. Nahon, D. Nandi, L. Poisson, and M. Hochlaf, Phys. Chem. Chem. Phys. **12**, 3566 (2010).
13   P. O'Keeffe, E. Gryzlova, D. Cubaynes, G. Garcia, L. Nahon, A. Grum-Grzhimailo, and M. Meyer, Phys. Rev. Lett. **111** (2013).
14   L. Nahon, G. A. Garcia, and I. Powis, J. Electron Spectrosc. Relat. Phenom. **204**, 322 (2015).
15   M. M. Rafiee Fanood, N. B. Ram, C. S. Lehmann, I. Powis, and M. H. M. Janssen, Nat. Commun. **6**, 7511 (2015).
16   M. Tia, B. Cunha de Miranda, S. Daly, F. Gaie-Levrel, G. A. Garcia, L. Nahon, and I. Powis, J. Phys. Chem. A **118**, 2765 (2014).
17   B. Cunha de Miranda, C. Alcaraz, M. Elhanine, B. Noller, P. Hemberger, I. Fischer, G. A. Garcia, H. Soldi-Lose, B. Gans, L. Vieira Mendes, S. Boyé-Peronne, S. Douin, J. Zabka, and P. Botschwina, J. Phys. Chem. A **114**, 4818 (2010).
18   G. A. Garcia, X. F. Tang, J. F. Gil, L. Nahon, M. Ward, S. Batut, C. Fittschen, C. A. Taatjes, D. L. Osborn, and J. C. Loison, J. Chem. Phys. **142**, 164201 (2015).
19   J. Kruger, G. A. Garcia, D. Felsmann, K. Moshammer, A. Lackner, A. Brockhinke, L. Nahon, and K. Kohse-Hoinghaus, Phys. Chem. Chem. Phys. **16**, 22791 (2014).
20   A. Bodi, P. Hemberger, D. L. Osborn, and B. Sztaray, J. Phys. Chem. Lett. **4**, 2948 (2013).
21   D. Felsmann, A. Lucassen, J. Krüger, C. Hemken, L.-S. Tran, J. Pieper, G. A. Garcia, A. Brockhinke, L. Nahon, and K. Kohse-Höinghaus, Z. Phys. Chem. **230** (2016).
22   B. Cunha de Miranda, G. A. Garcia, F. Gaie-Levrel, A. Mahjoub, T. Gautier, B. Fleury, L. Nahon, P. Pernot, and N. Carrasco, J. Phys. Chem. A **120**, 6529 (2016).
23   A. Lafosse, M. Lebech, J. C. Brenot, P. M. Guyon, O. Jagutzki, L. Spielberger, M. Vervloet, J. C. Houver, and D. Dowek, Phys. Rev. Lett. **84**, 5987 (2000).
24   X. Tang, X. Lin, W. Zhang, G. A. Garcia, and L. Nahon, PhysChemChemPhys **18**, 23923 (2016).
25   P. Brechignac, G. A. Garcia, C. Falvo, C. Joblin, D. Kokkin, A. Bonnamy, P. Parneix, T. Pino, O. Pirali, G. Mulas, and L. Nahon, J. Chem. Phys. **141**, 164325 (2014).
26   C. Joblin, L. Dontot, G. A. Garcia, F. Spiegelman, M. Rapacioli, L. Nahon, P. Parneix, T. Pino, and P. Bréchignac,  (submitted).
27   A. Bodi, J. Csontos, M. Kállay, S. Borkar, and B. Sztáray, Chem. Sci. **5**, 3057 (2014).
28   S. Daly, I. Powis, G. A. Garcia, H. Soldi-Lose, and L. Nahon, J. Chem. Phys. **134**, 064306 (2011).

[29]   L. Nahon, G. A. Garcia, H. Soldi-Lose, S. Daly, and I. Powis, Phys. Rev. A **82**, art. no. 032514 (2010).

[30]   I. Powis, S. Daly, M. Tia, B. Cunha de Miranda, G. A. Garcia, and L. Nahon, Phys. Chem. Chem. Phys. **16**, 467 (2014).

[31]   S. Hartweg, B. L. Yoder, G. A. Garcia, L. Nahon, and R. Signorell, Phys. Rev. Lett. **118**, 103402 (2017).

[32]   M. Tia, PhD Thesis, Université Paris-Sud, 2014.

[33]   A. T. J. B. Eppink and D. H. Parker, Rev. Sci. Inst. **68**, 3477 (1997).

[34]   L. Nahon, N. d. Oliveira, G. Garcia, J. F. Gil, B. Pilette, O. Marcouille, B. Lagarde, and F. Polack, J. Synchrotron Rad. **19**, 508 (2012).

[35]   B. Mercier, M. Compin, C. Prevost, G. Bellec, R. Thissen, O. Dutuit, and L. Nahon, J. Vac. Sci. Tech. A **18**, 2533 (2000).

[36]   S. Daly, I. Powis, M. Tia, G. A. Garcia, and L. Nahon, Int. J. Mass Spectrom. **376**, 46 (2015).

[37]   L. Nahon, G. A. Garcia, C. J. Harding, E. A. Mikajlo, and I. Powis, J. Chem. Phys. **125**, 114309 (2006).

[38]   W. M. Trott, N. C. Blais, and E. A. Walters, J. Chem. Phys. **69**, 3150 (1978).

[39]   S. H. Linn, Y. Ono, and C. Y. Ng, J. Chem. Phys. **74**, 3342 (1981).

[40]   Y. Ono, S. H. Linn, H. F. Prest, M. E. Gress, and C. Y. Ng, J. Chem. Phys. **73**, 2523 (1980).

[41]   P. J. A. Ruttink and P. C. Burgers, Org. Mass Spectrom. **28**, 1087 (1993).

[42]   P. C. Burgers, L. M. Fell, A. Milliet, M. Rempp, P. J. A. Ruttink, and J. K. Terlouw, Int. J. Mass Spectrom. **167**, 291 (1997).

[43]   I. Powis, in *Advances in Chemical Physics*, edited by J. C. Light (Wiley, New York, 2008), Vol. 138, pp. 267.

[44]   G. A. Garcia, L. Nahon, C. J. Harding, and I. Powis, Phys. Chem. Chem. Phys. **10**, 1628 (2008).

[45]   I. Powis, C. J. Harding, S. Barth, S. Joshi, V. Ulrich, and U. Hergenhahn, Phys. Rev. A **78**, 052501 (2008).

[46]   N. Borho and M. A. Suhm, Phys. Chem. Chem. Phys. **4**, 2721 (2002).

[47]   A. Maris, B. M. Giuliano, D. Bonazzi, and W. Caminati, J. Am. Chem. Soc. **130**, 13860 (2008).

## Figures
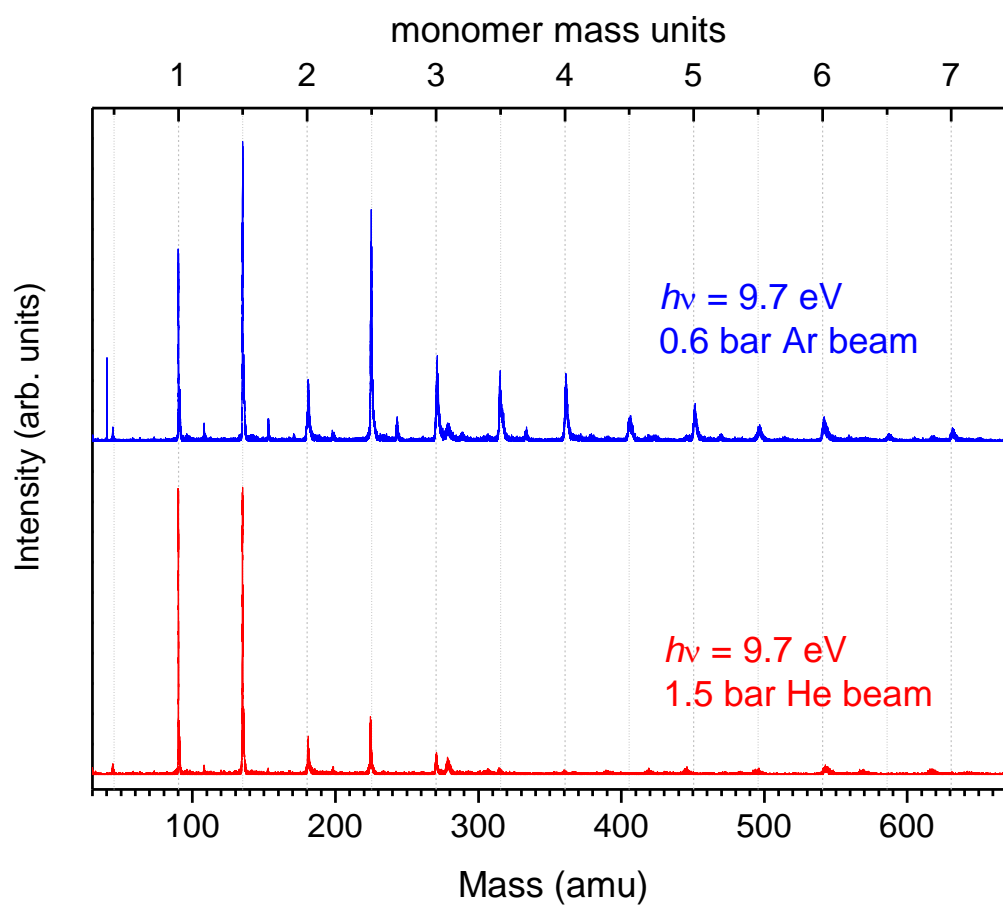


Fig 1. Ion time-of-flight (ToF) mass spectra of 2,3 butanediol recorded at 9.7 eV photon energy in He and Ar molecular beam clustering expansions. An alternative mass scale calibrated in monomer mass units (1 monomer=90.12 amu) is marked along the top axis.
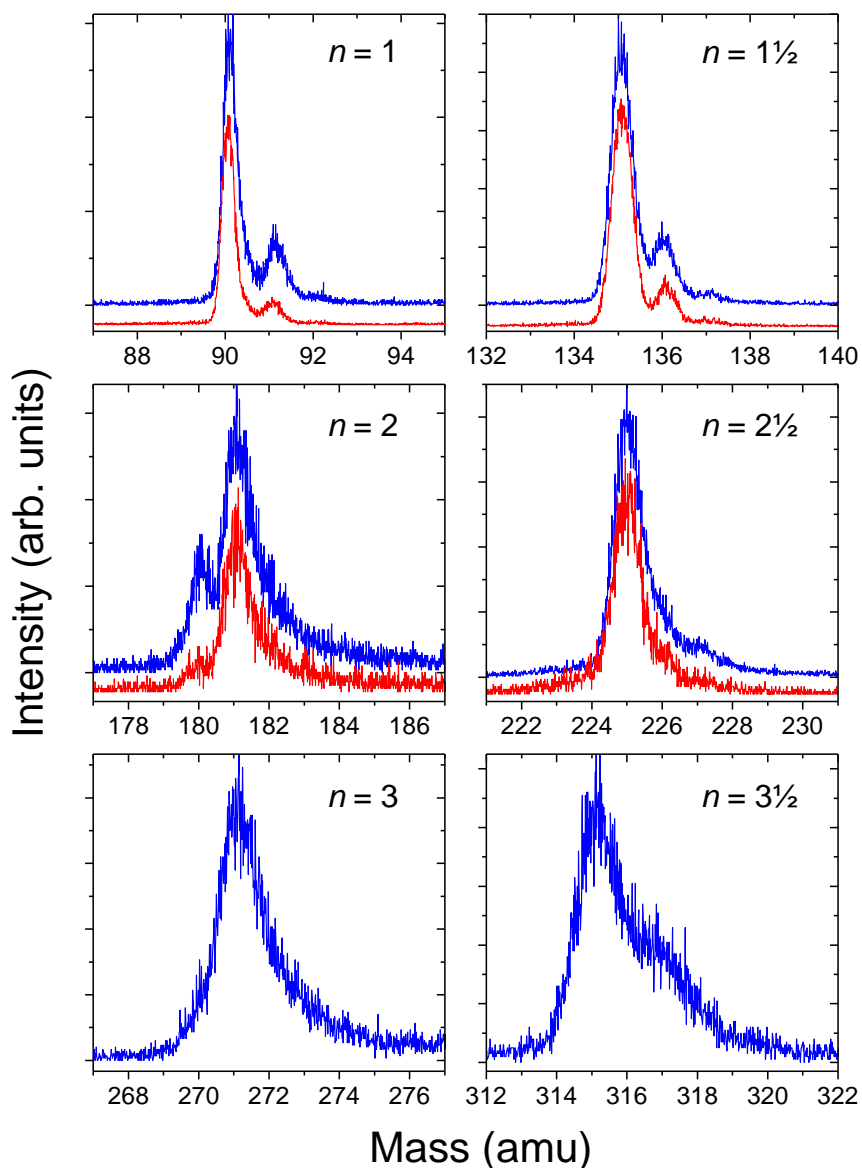
Fig. 2 Expanded $h\nu$ = 9.7 eV ion ToF mass spectra of the principal component peaks. The operating mode provided improved mass resolution at the expense of limiting electron energy resolution; consequently no selection on the coincident electron energy has been applied. Recorded with molecular beam nozzle backing pressures of 0.6 bar Ar (blue curve ) and 1.5 bar He (red curve) (as Fig. 1). For clarity a small vertical offset is applied between the He and Ar expanded ToF spectra. Cluster size is labelled as $n$, the number of monomer units in the cluster.
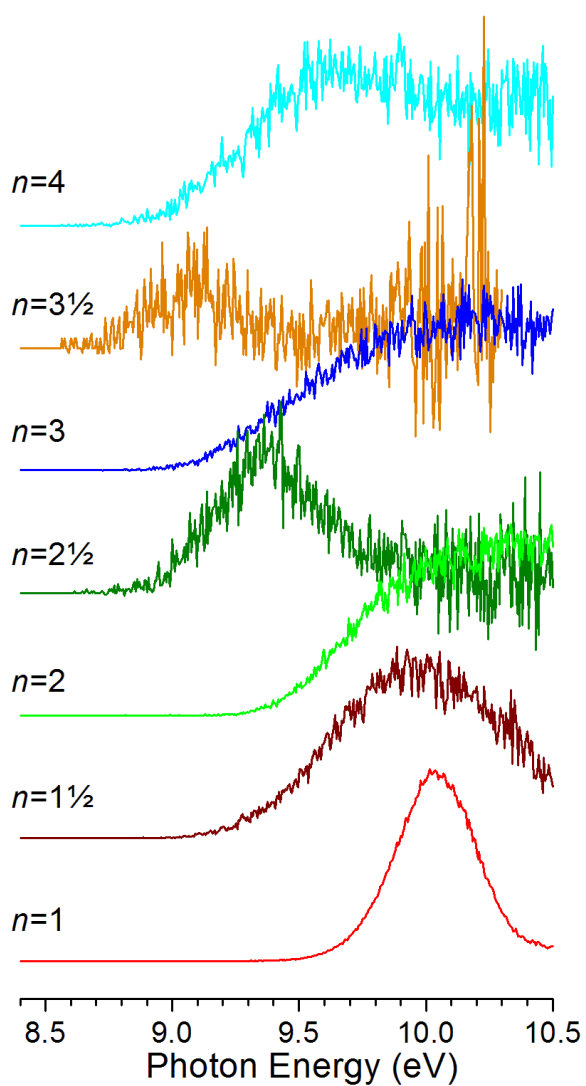
Fig. 3 Size-selected TPEPICO scans (size-selected TPES) taken in 0.6 bar Ar cluster beam conditions. The estimated threshold electron energy resolution was set as 50 meV to secure reasonable statistics. The individual traces have been normalized.
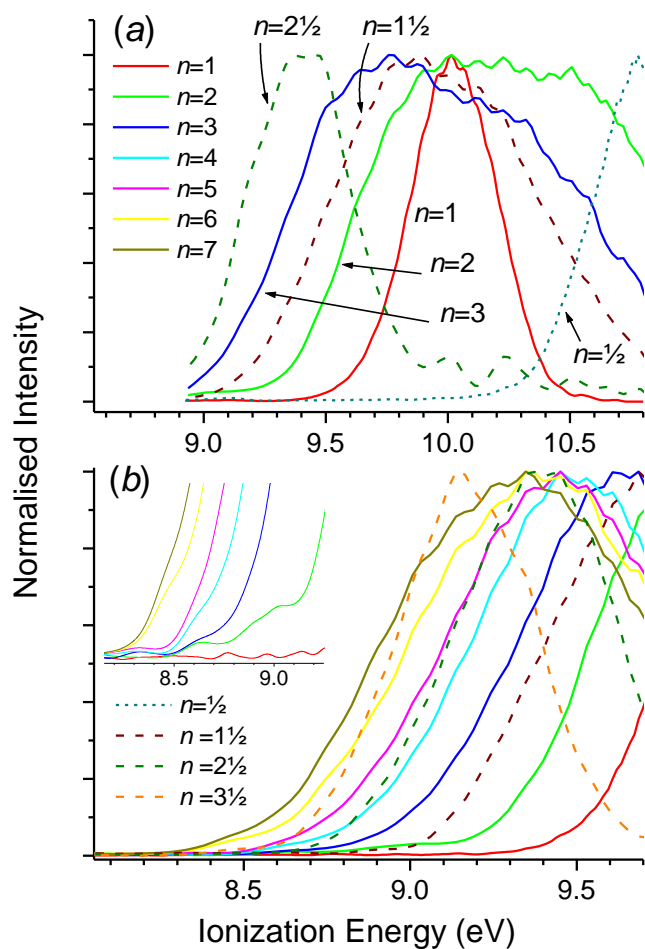
Fig 4 VMI PES of individually normalised, size-selected 2,3-butanediol clusters recorded in : (a) He clustering expansion (1.5 bar backing pressure) at $h\nu$=11.0 eV; (b) Ar expansion (0.6 bar backing pressure) at $h\nu$=10.0 eV. The inset here shows an expansion of the $n$-mer cluster threshold regions. The legends identifying cluster size apply in both panels.
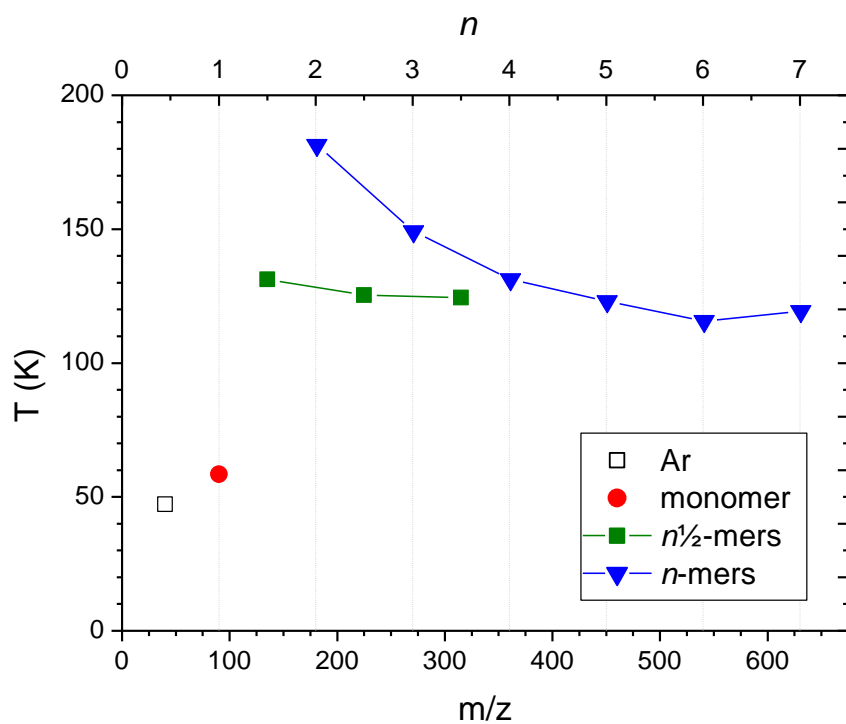
Fig. 5 Translational temperatures for ions produced in 0.6 bar Ar expansion and photon energy integrated from $h\nu$= 8.9—9.4 eV. The data was obtained by 3D ion momentum imaging using the DELICIOUS 3 spectrometer.[9]
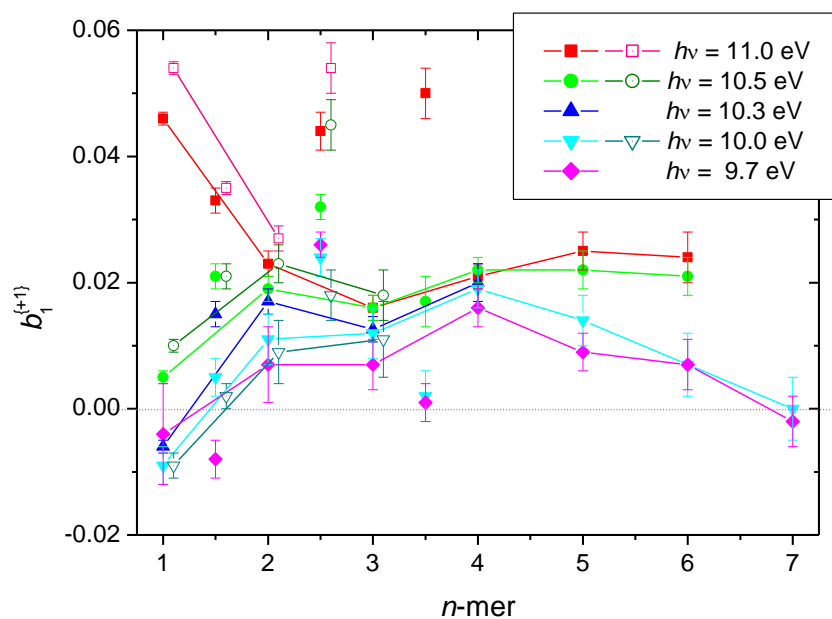
Fig 6 Size-selected PECD $b_1^{\{+1\}}$ parameters obtained as a weighted averaged over the associated VMI-PES band profiles. Straight lines joining the *n*-mer sequence values at a given photon energy are drawn to guide the eye, and exclude the (*n*+½)-mer results. Measurements made in a 0.6 bar Ar expansion are plotted with as solid symbols, those in 1.5 bar He with open symbols. The latter have been slightly displaced to the right for clarity.
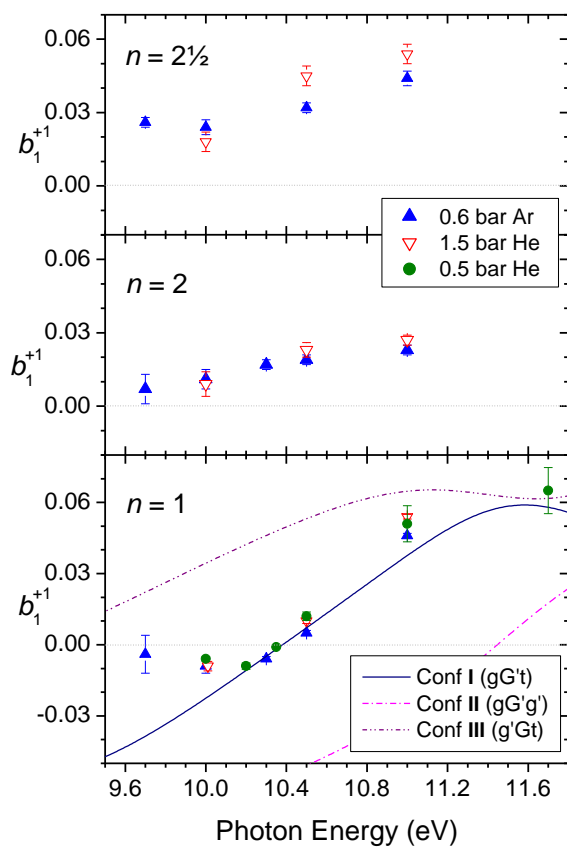
Fig 7 PECD $b_1^{\{+1\}}$ parameters, quantifying the chiral anisotropy in the photoelectron angular distribution, obtained for the $n=1$, and $n=2$, 2½ clusters. The values are weighted averages formed over the associated VMI-PES band. Measurements were made in clustering 0.6 bars Ar and 1.5 bars He expansions. Also shown are monomer PECD results in non-cluster forming 0.5 bar He expansion (Ref. [4]). Theoretical calculations for the lowest energy monomer conformations (**I – III**) taken from Ref [4] are added to the lower panel.
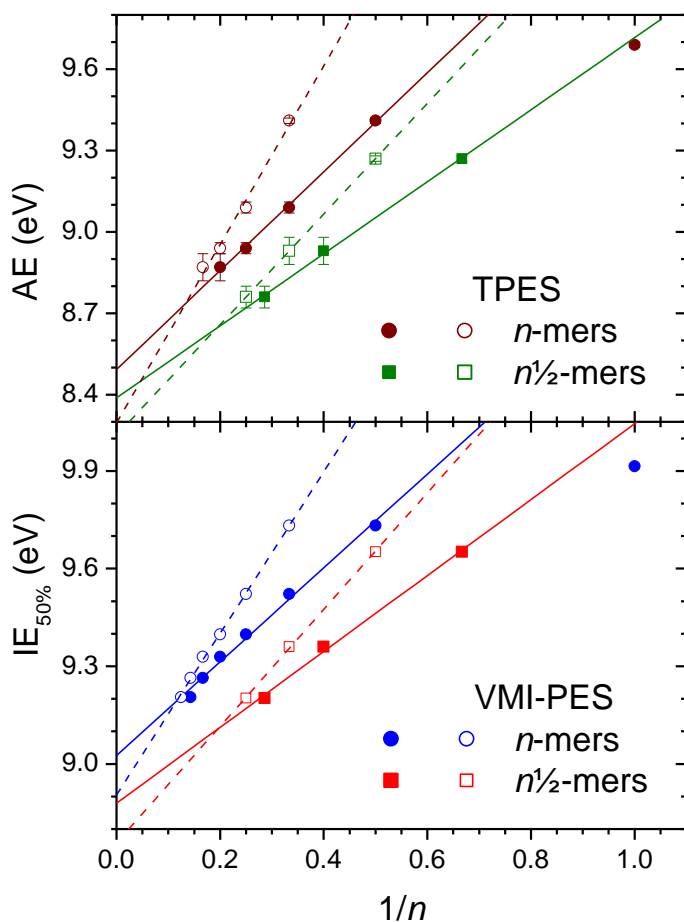
Fig 8 Size-selected *n*-cluster energies (solid symbols) plotted against $1/n$. Top panel are appearance energies from the TPEPICO/TPES data (Fig. 3 and Table 1). Bottom panel are ionization energies measured on the rising edge at 50% peak height of size-selected VMI-PES recorded at $h\upsilon=10.5$ eV. Straight lines are best fits through either the *n½*-mer or *n*-mer data (excluding *n*=1 which falls far off the straight line behaviour. The open symbols and dashed lines show the same data treatment with *n* increased to the next whole number (i.e. representing the smallest neutral cluster that could have been dissociatively ionized to $BD_n \cdot H^+$ or $BD_{n+½}^+$).
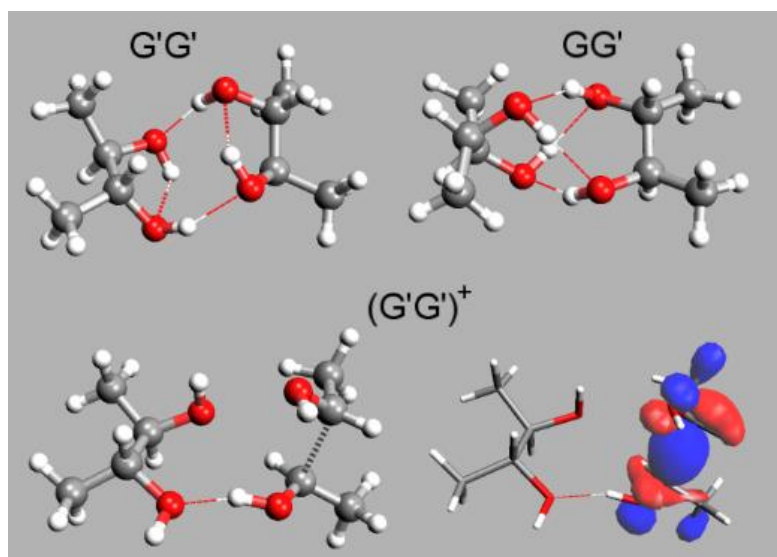
Fig 9. H-bond networks in neutral 2R,3R butanediol dimers consisting of two G' backbone monomer units (left, top) or a G' and G monomer (right top). The bottom row shows a cation G'G' geometry which has an extended (2Å) central C-C bond in the ionized moiety(left); while (right) the single occupied HOMO ion orbital can be viewed. The GG' ion (not shown) looks similar to the neutral.